Comprehensive Evaluation of commercially Scalable Atomic-layer-deposited Alumina Coating Impact on Full Cell Battery Performance Across Varied Test Conditions

Yue FENG,[1*] Runming Tao,[1] Kelsey Livingston,[1] Jaswinder Sharma[1], David A. Cullen,[2] Yu Lu,[1] Wheatley Steenman,[1] Markus Groner,[3] Arrelaine Dameron,[3] Georgios Polizos,[1] Jianlin Li[4*]

[1] Electrification and Energy Infrastructures Division, Oak Ridge National Laboratory, Oak Ridge, TN 37831, USA

[2] Center for Nanophase Materials Sciences, Oak Ridge National Laboratory, Oak Ridge, TN 37831, USA

[3] Forge Nano, Inc., Thornton, CO 80241, USA

[4] Applied Materials Division, Argonne National Laboratory, Lemont, IL 60439, USA

**Emails: jianlin.li@anl.gov; fengy1@ornl.gov*

1. Abstract

Atomic Layer Deposition (ALD) has emerged as a strategic enhancement method for lithium-ion battery (LIB) materials offering potential benefits and durability benefits for industrial battery production. However, the translation from laboratory achievements to commercial-scale applications has been limited. This study aims to bridge this gap by comprehensively evaluating the effects of commercially scalable Al_2O_3 ALD coatings using full pouch cell performance as a means to assess the ALD impact. We utilized large-scale slot-die coating techniques to ensure consistent electrode quality and tested four configurations of pouch cells to analyze the individual effects of ALD coating on anode and cathode electroactive materials. Our extensive testing matrix included long-term cycling, fast discharge, fast charge, leakage current, and high voltage tests. While at lower C-rates (<~1C), the influence of Al_2O_3 coatings on cell performance is not significant. Fast charging conditions reveal that the anode ALD coating significantly enhances performance via a passivating effect, while on the cathode, it is detrimental, potentially due to increased resistance of the thin interfacial layer formed during the ALD processing. Leakage current and high-voltage tests show that the application of ALD coatings on either anode or cathode effectively minimizes side reactions at the electrode-electrolyte interface. Additionally, ALD coatings significantly mitigate concentrated and localized lithium plating on the anodes. These insights provide a valuable understanding of the potential of ALD technologies in LIB manufacturing to tailor cell performance, paving the way for safer, more efficient, and cost-effective battery solutions.

2. Introduction

The global demand for lithium-ion batteries (LIBs) is expanding rapidly, primarily fueled by the growing commercial vehicle and passenger transportation sectors. With the continuous rise of the electric vehicle (EV) market, LIB technology faces critical challenges that need to be addressed. These challenges include extending the driving range [1, 2], improving the fast charging and discharging capabilities [3, 4], and enabling high-capacity and high-voltage cathode materials [5, 6]. Additionally, improving battery efficiency, reliability, safety, and developing cost-effective manufacturing processes [7, 8] are essential to meet the growing demands.

In a typical LIB system, the main components include anode and cathode electrodes, separators, electrolyte, and current collectors. During cycling, issues with any of these components can lead to battery failure. Cathodes frequently encounter challenges such as the dissolution of metal ions, structural disorder, side reactions with electrolyte, and particle cracking [9-11]. On the anode side, common issues involve the continuous formation of solid electrolyte interphase (SEI) layers and the growth of lithium dendrites [12, 13]. These problems collectively lead to reduced battery capacity and increased internal resistance, thereby accelerating the degradation process [14, 15]. To tackle these complex challenges, researchers are actively pursuing effective solutions aimed at prolonging the lifespan and enhancing the performance of LIBs. For example, discovering advanced electrode materials, optimizing electrolyte formulations, investigating solid-state electrolytes, and employing interfacial and nano-engineering techniques in electrode design. Among all the strategies, modifying the surface of electrode materials has emerged as a particularly promising approach. By engineering protective layers or altering the electrode surfaces at the microscopic level, it's possible to alleviate the negative impacts of electrode degradation and prevent harmful reactions between the electrodes and electrolytes. Various coating techniques are applied to electroactive materials, such as sol-gel [16, 17], pulsed laser deposition (PLD) [18], physical vapor deposition (PVD) [19], and chemical vapor deposition (CVD) [20]. In addition, carbon pitch coatings are applied to graphite using high-temperature processes. [21] However, these methods frequently face challenges in attaining precisely controlled thicknesses and uniformity, which can result in thick, non-uniform films, with stress and cracks forming on the film surface, which in turn affect the transmission of ions and electrons [16, 22]. Atomic Layer Deposition (ALD) distinguishes itself by enabling the growth of ultra-thin films with atomically precise thickness control and excellent conformality. ALD coatings can be grown on a wide range of materials via self-limiting surface reactions [23, 24], thereby ensuring good

uniformity and strong chemical bonding to the substrate, and with very thin films often providing similar benefits as thicker films deposited by other methods.

Various ALD films have been explored for coating LIB electroactive materials [25], including metal oxides (Al_2O_3 [26-28], ZnO [29], ZrO_2 [30], etc.), and metal fluorides (LiF [31], AlF_3 [32], etc.). Among all the coating materials, Al_2O_3 is the most extensively explored and well-established material due to its low cost, ease of deposition, and excellent performance [26]. Typically, the Al_2O_3 ALD coating is produced using trimethylaluminum (TMA) and H_2O as precursors [24]. An Al_2O_3 coating on cathode materials can i) suppress structure and chemistry changes on the particle surface (transition metal dissolution, oxygen loss, phase transition) [26, 33]; ii) reduce the oxidative decomposition of electrolyte and improve the stability of the cathode–electrolyte interphase (CEI) layer [34]; and iii) prevent the particle pulverization [33]. Similarly on anodes, the Al_2O_3 ALD coating can offer multiple benefits: i) improving the stability of the SEI layer by reducing the electrolyte decomposition [35, 36]; ii) suppressing the formation of lithium dendrites [37]; iii) better accommodating the volume expansion/contraction during charging and discharging, thus avoiding particles pulverization and loss of electronic conductivity in silicon-based anodes [38].

Despite numerous experimental studies and supporting theoretical work about the benefits of ALD coatings on electrode performance, many remain academic, failing to transition beyond lab-scale experiments. High throughput, such as roll-to-roll process, has been rarely reported [39]. Often, the exceptional performance reported in scientific literature is assessed under conditions that are not aligned with the practically relevant processing conditions and testing conditions. Challenges include scalability & cost concerns of certain ALD processes, impractical mass loadings of electrodes, and focusing only on testing one electrode (anode or cathode) in half-cell configurations. Additionally, experiments are often conducted on a small scale in coin cell setups, with limited testing conditions that do not mirror practical demands. Hence, there is a significant gap between laboratory achievements and the commercialization of ALD-coated electrodes that must be addressed. In this paper, we aim to bridge the gap between laboratory and commercial applications by conducting comprehensive evaluations of scalable Al_2O_3 ALD coating impacts on full-cell battery performance in various test conditions. Our approach involves applying Al_2O_3 ALD coatings via commercially scalable powder ALD processing equipment from Forge Nano (up to tons per day) to both anodes and cathode powders, and implementing large-scale electrode coatings (hundreds of feet) using slot-die coating for consistent quality. We conducted tests on four configurations of single-layer full-pouch cells, featuring variations in coated and uncoated anodes and cathodes, each in triplicate, to specifically analyze the individual effects of ALD

coating on either the anode or the cathode in the full cells. A comprehensive testing matrix, covering long-term cycling, fast discharge, fast charge, and high voltage, was developed and employed on these pouch cells. Our study aims to shed light on the potential of ALD surface modifications to revolutionize LIB manufacturing, offering a pathway to safer, more efficient, and cost-effective battery technologies.

3. Experimental

I. Coating process:

The Al_2O_3 ALD coatings were deposited on lithium nickel manganese cobalt oxide ($LiNi_{0.8}Mn_{0.1}Co_{0.1}O_2$, NMC811) and SLC1520T graphite powders, purchased from Gelon Lib Co., Ltd. and Superior Graphite, respectively. The ALD coating process was performed by Forge Nano in one of their large powder ALD coating tools. In this work, batches of anode and cathode powders, each ranging between 6-10 kg, were coated with two cycles of Al_2O_3 ALD, utilizing trimethylaluminum (TMA) and water in a fluidized bed reactor. The powders were fluidized using nitrogen gas, and pre-dried at 180°C overnight. During each ALD cycle, TMA and water vapors were sequentially introduced until residual gas analyzer readings indicated the completion of the respective surface chemical reactions, as evidenced by breakthrough of the reactant chemical species, along with a rapid drop in the byproduct methane. Each dosing step was followed by a purging phase to ensure the removal of excess reactants and byproducts. After coating, the powders were cooled and vacuum sealed under nitrogen in a foil bag to limit moisture and air exposure during transport and storage. The pristine materials are referred to as uncoated-NMC811 and uncoated-graphite, while the Al_2O_3-coated samples are labeled as ALD@NMC811 and ALD@Graphite.

II. Electrode preparation:

Cathode slurries were composed of 90 wt% of either coated or uncoated NMC811, 5 wt% carbon black (C65, Denka), and 5 wt% polyvinylidene difluoride (PVDF, Solvay 5130) in N-methylpyrrolidone (NMP, Sigma-Aldrich). Similarly, anode slurries were formulated with 92 wt% of either coated or uncoated graphite, 2 wt% carbon black (C65, Denka), and 6 wt% PVDF (KUREHA 9300), also in NMP. The mixing process for both slurries was conducted using a planetary mixer (Ross PDM – 1/2). Similar slurry fabrication process can be found in our previous publication [40].

The electrodes were coated onto either aluminum or copper foil (MTI Corporation) using a pilot-scale slot-die coater (Frontier Industrial Technology). The total mass loading of the cathode and anode is 11.1 mg/cm^2 and 7.1 mg/cm^2, respectively. For all the mass loading, the electrode balance (N/P ratio) was maintained at approximately 1.12 to 1.17. Post-coating and drying, the electrodes were calendered to ~35% porosity. Subsequently, all electrodes were subjected to a secondary drying process at 115 °C under vacuum conditions to prepare them for cell assembly.

III. Coin cell and pouch cell fabrication:

Half coin cells (CR2023) were assembled with electrodes precisely cut to a diameter of 12.7 mm, in a glove box under Ar atmosphere, using Celgard 2400 separator and Gen 2 electrolyte (1.2 M $LiPF_6$ in 3:7 wt% ethylene carbonate/ethyl methyl carbonate).

For single-layer pouch cell assembly, cathodes and anodes were cut to dimensions of 8.4 cm x 5.6 cm and 8.6 cm x 5.8 cm, respectively. All pouch cells with an approximate capacity of 85.5 mAh were assembled in a dry room environment maintained at relative humidity lower than 0.3%. These cells utilized Celgard 2400 separators and were filled with Gen 2 electrolyte. The electrolyte volume factor was 1.9, same as our former publications [41]. Prior to testing, all cells underwent a formation process involving three cycles at C/10, ranging from 3 to 4.2 V.

IV. Electrochemical testing procedure

The rate performance of all electrodes was evaluated using a half-coin cell configuration. For the NMC811 half-cell, the test protocol included a constant current charge at C/3 to 4.3 V followed by a constant voltage charge at 4.3V with a trickle current of C/20 and discharge at C/5, C/3, C/2, 1C, 2C, 4C to 3.0 V for 5 cycles each, respectively, where 1C=180 mA/g_{NMC}. For the graphite half-cells, discharge followed a constant charge and constant voltage (CCCV) pattern at C/3 to 5 mV, with a trickle current of C/20. Charging took place at C/5 to 4C, again, for 5 cycles each, operating within a voltage range of 5 mV to 1.5 V.

To assess the effect of the Al_2O_3 coating on the performance of full cells, 48 single-layer pouch cells in four configurations—UCUA (uncoated cathode & uncoated anode), UCCA (uncoated cathode & coated anode), CCUA (coated cathode & uncoated anode), and CCCA (coated cathode & coated anode)—were subjected to a series of tests under five different testing protocols. These include USABC cycling (0.33C/-0.33C), high-power discharge cycling (0.5C/-1C), XFC cycling (4C/1C), leakage current testing at high voltage, and high voltage testing (0.33C/-0.33C at 4.4V).

The specifics of these protocols are detailed in Table 1. Notably, Test 5 was conducted after Test 4 and performed on the same cells.

All the tests of coin cells and pouch cells were conducted in a temperature chamber (ESPEC) at 30 ºC using a Maccor battery cycler (Series 4000).

Table 1. Electrochemistry testing protocols

Protocol number	Testing procedure
Test 1	0.333C/-0.333C 4.2V upper cutoff voltage (UCV) with voltage hold of 10-min or current ≤ 1/20C USABC long term cycling. (3 duplicates for each)
Test 2	0.5C/-1C 4.2V UCV with voltage hold of 10-min or current ≤ 1/20C normal charge. (3 duplicates for each)
Test 3	4C/-1C 4.2V UCV with voltage hold at 4.2V fast charging while limiting the total charge time to be 15 min. (3 duplicates for each)
Test 4	Measure leakage current at 4.6V: Charge the pouch cells to 4.6V at 0.333C and record the leakage current during 2-days relaxation
Test 5	High voltage testing: 0.333C/-0.333C 4.4V with voltage hold of 10-min or current ≤ 1/20C UCV cycling. (3 duplicates for each) This test was started on the same cells that completed Test 4.

The electrochemical impedance spectra (EIS) were measured at the end of cycling, in the frequency range from 500 kHz to 10 mHz using a VMP-3 potentiostat (Biologic, France), at 30 ºC.

V. Material and electrode characterization:

The composition, crystallinity, and morphology of the electrode materials were analyzed using a suite of techniques: elemental analysis via inductively coupled plasma optical emission spectroscopy (ICP-OES, PerkinElmer Optima 8000, US), X-ray diffraction (XRD, PANalytical X'pert PRO, UK), scanning electron microscopy (SEM, Thermo Fisher Scientific, US), and the Talos F200X transmission electron microscope (TEM, Thermo Fisher Scientific).

4. Results and discussions

I. Material characterization

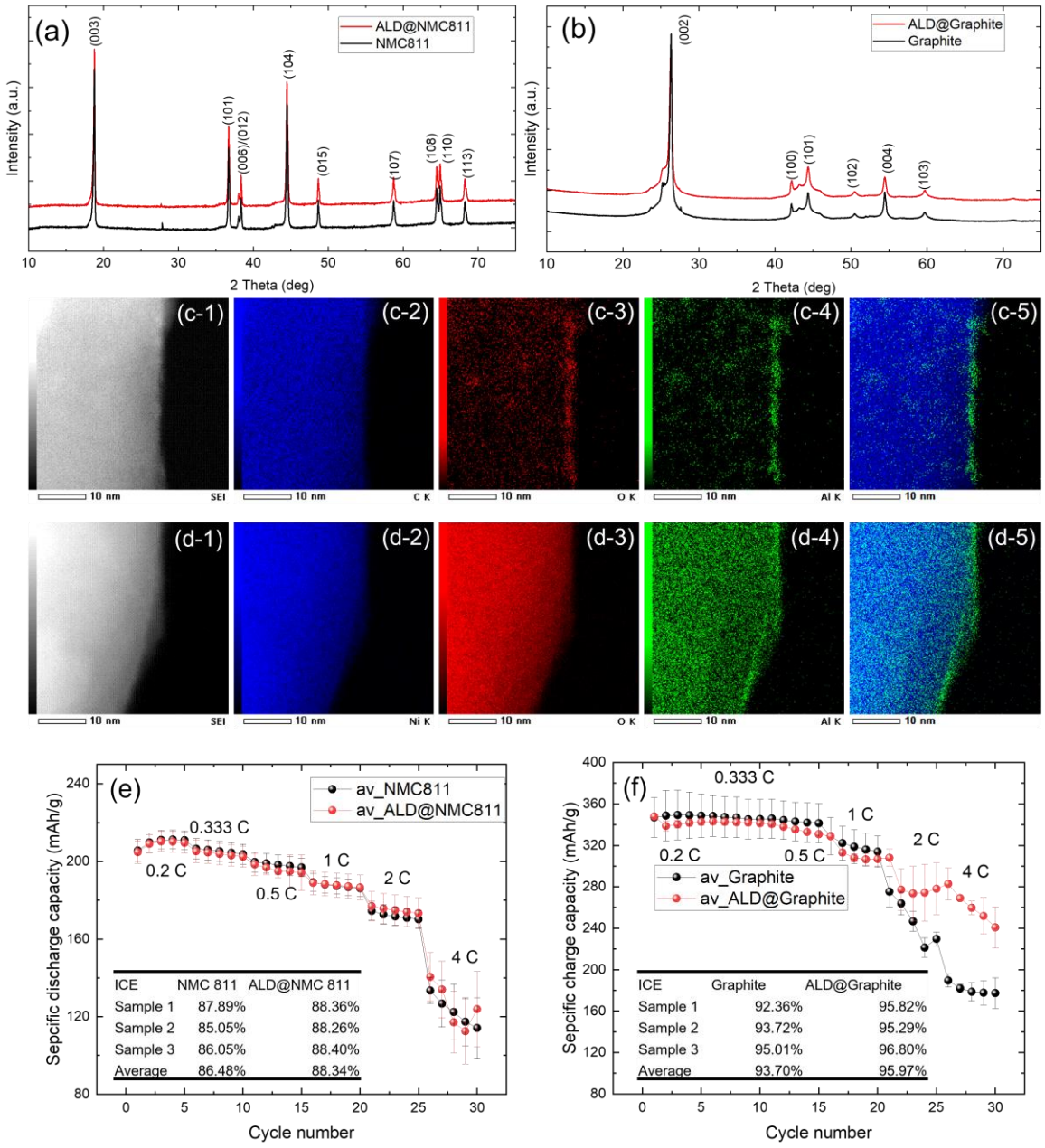

Figure 1. X-ray diffraction patterns of ALD coated and uncoated NMC811 (a), graphite (b) powders. TEM-EDX analysis on the ALD@Graphite (c) and ALD@NMC811 (d). Discharge rate capability of ALD-coated vs. uncoated NMC811

(e), and charge rate capability of ALD-coated vs. uncoated graphite (f), across current densities from 0.2C to 4C. Five cycles per current density; three coin cells tested per material. The ICE of all the samples are presented in the tables.

Figure 1a displays the XRD patterns of both the ALD-coated and uncoated NMC811 powders, in a 2θ range from 10° to 80°. All the primary peaks are labeled in the figure, and they align well with the NMC811 reference [42, 43]. The split peaks at (006)/(102) and (108)/(110) indicate that the two materials are highly crystallized [44, 45]. There is a negligible difference between the XRD patterns of the coated and uncoated materials, indicating that the crystal structure of NMC811 remains unchanged after the ALD coating process. Additionally, no prominent Al_2O_3 peaks are detected in the ALD-coated material, implying a minimal amount of amorphous Al_2O_3 coating [46]. Similarly, no change in structure is observed and no Al_2O_3 peaks are detected for the graphite powder (Figure 1b).

Figure S1 presents the SEM images of the ALD-coated cathode (a) and anode (d). The corresponding EDX mapping results for these are shown in Figure S1b and 1e, respectively. A minuscule atomic percentage of Al elements is detected on the ALD electrodes: 0.14% on the cathode and 0.02% on the anode. The ALD-coated anode and cathode powders were analyzed using TEM-EDX, as depicted in Figure 1c&d. This analysis confirmed the successful application of an Al_2O_3 layer on NMC811 and graphite particles, with an apparent thickness of approximately 1-2 nm for both. Notably, the coating on the NMC powder appears more uniform and continuous than that on the graphite. The Al content of the Al_2O_3 coatings of both the anode and cathode powders were quantified using plasma-optical emission spectroscopy (ICP-OES), with the findings presented in Table 2. Both values are consistent with the expected ALD growth per cycle (GPC) of ~0.11nm/cycle for the TMA/water process. The NMC cathode powder aluminum content of 170 ppm, with a 0.29 m^2/g surface area, corresponds to ~0.3 nm of alumina, while on the graphite anode, it is somewhat lower at ~0.2 nm, perhaps attributable to slower nucleation on graphite. The layers appear thicker in the TEM-EDX, likely due to the formation of a mixed layer, such as LiAlOx or LiAlMOx [25, 27], and perhaps also due to surface roughness or smearing during cross sectioning.

Table 2. Analysis of Al_2O_3 coated cathode and anode powders.

Substrate	Surface area BET (m^2/g)	Moisture (ppm)	Al_2O_3 ALD coating	Al (ppm) ICP-OES	Calc. Al_2O_3 thickness (nm)

Gelon NMC 811	0.29	36	2 cycles	170	0.3 nm
Superior graphite SLC1520T	0.84	2	2 cycles	42	0.2 nm

II. Baseline of the ALD coated and uncoated active materials rate capability.

Figures 1e and f illustrate the discharge rate capability performance of uncoated and ALD-coated NMC811 (a), charge rate capability of uncoated and ALD-coated graphite (b) electrodes. Coin cells were assembled using Li metal as the counter electrode. All specific discharge capacity values depicted in the figure represent the average from three coin cell tests. First, all electrodes exhibited exemplary performance, on par with other commercial powders [47]. For the cathodes, both the uncoated and ALD-coated NMC 811 demonstrate similar performance from C/5 to 4C. The capacity gradually diminishes from ~215 mAh/g to ~130 mAh/g. For the anode material, the ALD coating demonstrates an improvement in performance at higher C-rates. At lower C-rates (C/5, C/3, C/2, and 1C), the difference in charge capacity is not significant, with ALD@Graphite showing a slightly lower capacity that is negligible compared to the uncoated graphite. However, at high C-rates, the ALD@Graphite shows a 14% increase at 2C, and a notable 44% increase at 4C compared to the uncoated graphite. Additionally, the ALD@Graphite displays an initial coulombic efficiency (ICE) of 95.97%, a 2% improvement over the uncoated one (93.7%). This suggests that the ALD coating reduces irreversible capacity loss during the initial cycle. In summary, the ALD coating seems more beneficial at high rates on the anode.

III. Effects of ALD coatings on full cells under various testing conditions

Figure 2 displays the specific discharge capacity (average of 3 cells) and capacity retention (average of 3 cells) for cells with four different configurations, evaluated under testing protocols 1 (a, b), 2 (c, d), 3 (e, f), and 5 (i, j). The capacity retention is calculated by the discharge capacity divided by the highest discharge capacity among all the cycles (usually in the first several cycles).

In Test 1 where the cells were charged and discharged at C/3, all cells exhibited promising performance. Even after 1,000 cycles, each cell maintained a discharge capacity above 140 mAh/g (Figure 2a). Within the initial 100 cycles, the UCUA configuration exhibits a slightly higher discharge capacity (~185 mAh/g), whereas the CCCA demonstrates a marginally lower capacity (~178 mAh/g). As cycling progresses, the discharge capacity of UCUA declines a little bit more

rapidly, while the other three configurations display a lower capacity degradation. In Figure 2b, the UCCA, CCUA, and CCCA configurations (all involving ALD in at least one electrode) demonstrate an 80% capacity retention after 1,000 cycles, whereas the UCUA (no ALD coating) exhibits a slightly lower retention at 75%. In the inset of Figure 2b, the capacity retention during the initial 25 cycles is detailed. Even after formation, all cells, except CCCA, experience a capacity increase within the first 10 cycles, with UCUA registering the largest rise at 2.5%. This gradual capacity rise in the early stages of Li-ion battery cycling is a commonly observed phenomenon [48-52]. Though it may seem beneficial, such behavior in practical settings can lead to operational instability in battery systems and, in some cases, may even result in accidents. Although numerous previous studies have explored the origins of this behavior, a comprehensive understanding of the underlying mechanism remains limited [53]. The mitigation of this undesirable capacity rise may be attributed to better electrolyte wettability of the ALD-coated electrodes, reducing the electrolyte distribution time (similar to that evidenced by coated separators) [54]. In CCCA cells, where both the cathode and anode are ALD-coated, this characteristic capacity increase is suppressed, potentially offering operational advantages in industrial applications. Figure S2 illustrates the charge and discharge voltage profiles of four-configuration cells at various stages – during formation, and at the 50^{th}, 500^{th}, and 950^{th} cycles – as tested under protocol 1. In the UCUA voltage profile (Figure S2a), the charge/discharge capacity during formation (red) is smaller than in the 50^{th} cycle. Whereas for the three involving ALD coatings, the formation cycle shows the highest capacity.

The effect of ALD coating on high-rate performance was investigated in Test 2 where the charge and discharge rates were increased to 0.5C and 1C, respectively. Figure 2 c-d illustrates the discharge capacity and capacity retention across the four cell configurations. Similar to the results observed in Test 1, all cells maintain a discharge capacity above 140 mAh/g after 1,000 cycles. Furthermore, each cell maintains approximately 80% capacity retention after cycling, reflecting the high quality of the electrode materials and the cell assembly process. Across all configurations, the CCUA exhibits marginally higher capacity retention throughout the cycling, whereas the CCCA consistently shows a slightly lower capacity. When looking at the capacity retention at the first 25 cycles (the inset in Figure 2d), similar to that observed in Test 1, capacity increase is observed in the first 10-15 cycles in UCUA, UCCA, and CCUA, but not CCCA. The detailed voltage profile of all cells during formation, 50^{th}, $500^{th,}$ and 950^{th} is shown in Figure S1. The UCUA exhibits the lowest discharge capacity during formation. These observations support the idea that electrodes with ALD coating can potentially shorten electrolyte wetting times. Overall, the test results from Test 1 and Test 2 show no significant differences, suggesting that the ALD coating does not

markedly impact performance under these testing conditions. This aligns with the results from the half-cell Rate Capability Cycling (RCC) tests, which also indicate no substantial enhancement from ALD coating at low C-rates. The primary advantage observed from ALD coating in both Test 1 and Test 2 is improved wettability, which contributes to reduced electrolyte wetting time.[55, 56]

Since the ALD coating showed limited impact on low to medium-rate performance, a fast charge test, where the charge and discharge rate were set at 4C and 1C, respectively, was performed as Test 3. Significant differences are observed among the four cell configurations, as depicted in Figure 2e&f. The UCCA configuration exhibits the most promising performance, maintaining over 150 mAh/g (~87% capacity retention) after 1000 cycles. In contrast, surprisingly, the CCUA displays the poorest performance, with a rapid capacity decline in the initial 100 cycles and stabilizing thereafter (75% capacity retention after 1000 cycles). As depicted in Figure S2 i-l, from the 50th cycle onward, the CCUA cell (Figure S2k) reaches 4.2V significantly faster than the other cells during 15-minute charging. As for UCUA, its capacity steadily decreases, showing 82% capacity retention after 1000 cycles, positioning it between UCCA and CCUA. These results suggest that during fast charging in the full cell, the ALD coating on the anode has a beneficial effect, whereas the coating on the cathode appears to have negative impacts. This may be attributed the amorphous Al_2O_3 coating acting as an insulating layer, which introduces decreased electronic conductivity to the cathode, consequently accelerating electrode degradation under fast charge conditions [57]. Conversely, the ALD coating on the anode acts as a preformed SEI, offering protection during fast charging[56]. The post-mortem characterizations and impedance measurements discussed in Section IV strongly support these arguments.

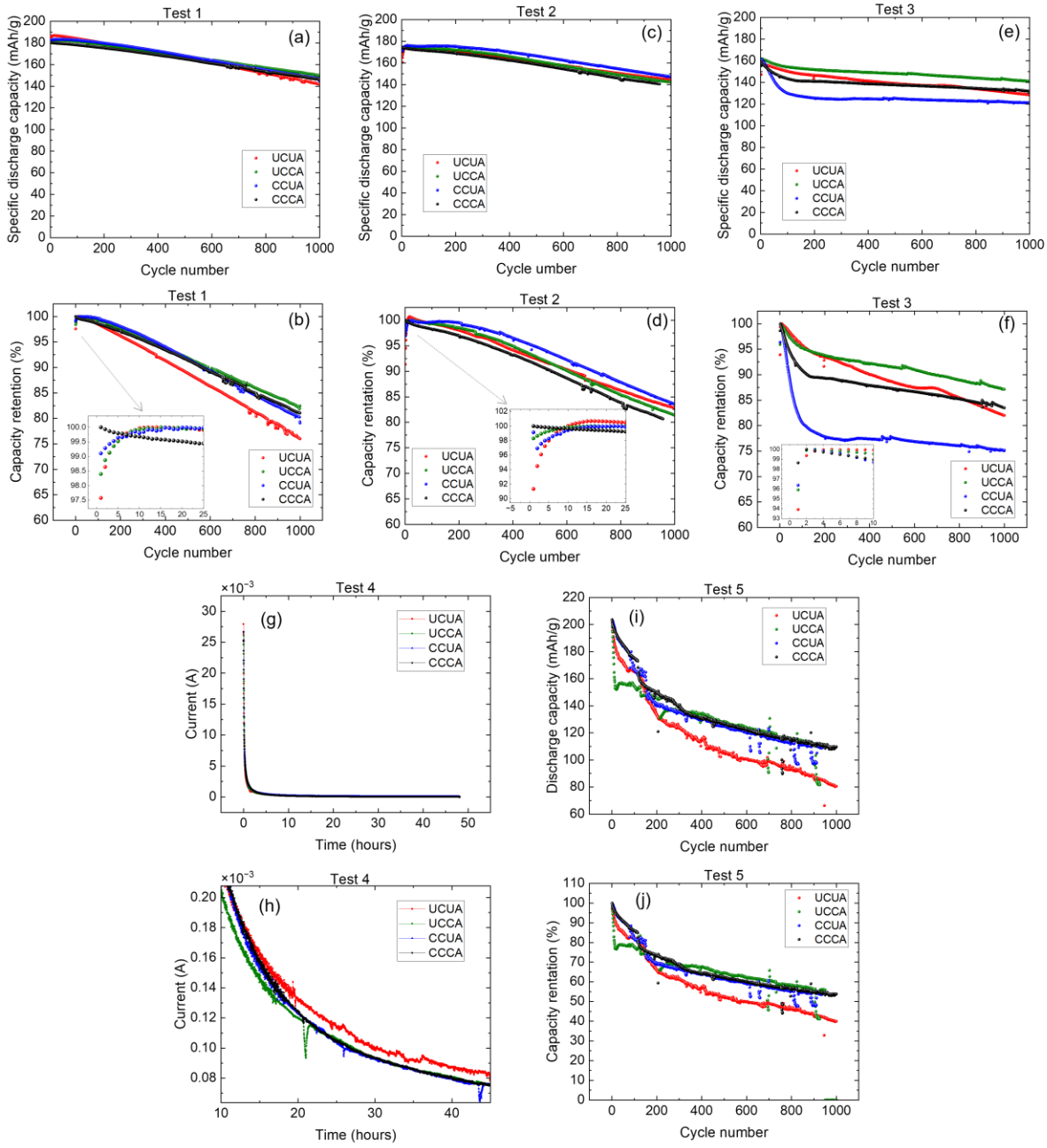

Figure 2. Specific discharge capacity (a, c, e, i) and capacity retention (b, d, f, j) of four-configuration pouch cells (UCUA, UCCA, CCUA, CCCA) tested by testing protocol 1, 2, 3 and 4. (g) Current profiles over time for pouch cells with four different configurations, tested under protocol 4. A magnified view of the profiles between 10-45 hours is presented in (h).

In Test 4, the leakage currents at a high voltage of 4.6V for four types of full pouch cells were monitored over two days, as shown in Figure 2g and h. While no significant differences are initially apparent in Figure 2h, a closer examination from 10-hour in Figure 2h, reveals that cells with ALD-coated electrodes (UCCA, CCUA, CCCA) exhibit lower leakage currents at 4.6V compared to those in the UCUA configuration. This observation indicates reduced side reactions at high voltages in cells where the electrodes are protected by ALD coating. Following Test 4, Test 5 was subsequently performed on the same cells. Differing from Test 1, the upper cutoff voltage was increased from 4.2V to 4.4V in Test 5. The resulting discharge capacity and capacity retention are depicted in Figure 2i and j. Notably, compared to the UCUA, the three cells with ALD coatings (UCCA, CCUA, CCCA) exhibit enhanced performance at the higher voltage. All three of these cells demonstrate over 50% capacity retention after 1000 cycles, while the UCUA maintains only about 40% of its capacity after cycling. Among all the cells, the CCCA cell displays the most stable performance throughout the 1000 cycles, suggesting that the ALD coating on both the anode and cathode is advantageous at higher voltages.

To examine the polarization behavior of different cell configurations, the average voltage difference between charging and discharging (ΔV) over 1000 cycles in Tests 1, 2, 3, and 5 was calculated and illustrated in Figure 3. Throughout all the tests, there is an observed increase in ΔV over time, attributable to heightened polarization, a result of electrode degradation. Consistent with expectations, in Tests 1 and 2, which involve relatively lower cycling C-rates, the four cell types show no marked differences. Specifically, in Test 1, under the mildest cycling conditions, the smallest ΔV is recorded among all tests, beginning at around 0.05V and increasing to approximately 0.15-0.18V after 1000 cycles. Meanwhile, in Test 2, ΔV rises from 0.1V to about 0.20-0.22V over 1000 cycles. With the increase of C-rate or voltage limit during cycling, notable differences emerge among the four cells, as demonstrated by the results of Tests 3 and 5. In Test 3 (Figure 3e), with the fast charge protocol (4C/-1C), the polarization behavior increases significantly compared to the first 2 tests. Particularly, the CCUA cell exhibits the highest polarization during the initial 300 cycles, but it stabilizes afterward, suggesting a rapid electrode degradation in the early stages. Conversely, the UCUA starts with a ΔV comparable to that of UCCA and CCCA in the first 300 cycles. However, its ΔV steadily and more rapidly increases in subsequent cycles, resulting in the highest polarization of all cells after 1000 cycles. In Test 5 (Figure 3g), carried out under high voltage conditions, a marked polarization (from 0.1V to approximately 0.45V) is observed, suggesting rapid electrode degradation at high voltage testing. Among all the cells, CCCA demonstrates the lowest polarization over the cycles, while UCUA shows the greatest. This observation implies that ALD coating on either the anode or the cathode

significantly improves cycling performance under high-voltage conditions. All these results are in good agreement with the observed cycling performance. Subsequent post-mortem characterization will offer deeper insights into understanding these behaviors.

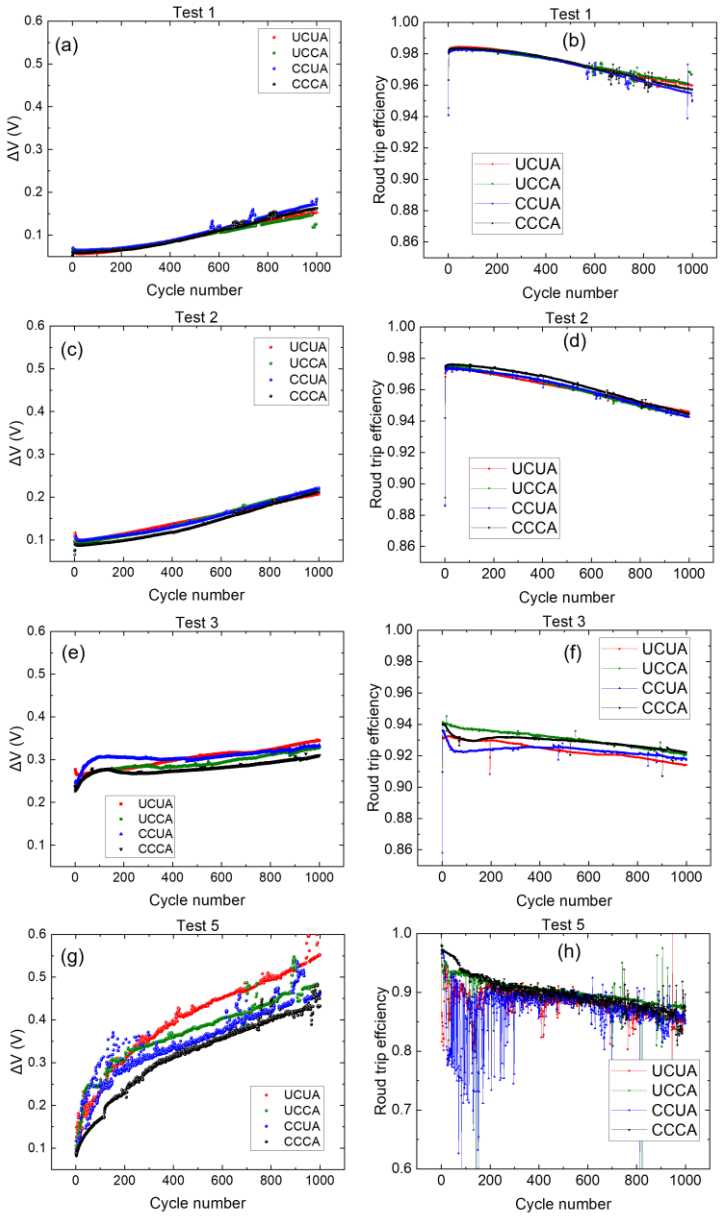

Figure 3. Average potential differences between charge and discharge for pouch cells with four different configurations phases are presented in a, c, e, g. Round trip efficiency of four-configuration pouch cells under testing protocols 1, 2, 3 and 5 are shown in b, d, f, h.

The Round-Trip Efficiency (RTE), calculated by normalizing the discharge energy by charge energy, is plotted for all the tests in Figure 3. The RTE trends align closely with polarization behavior, given that RTE is significantly affected by energy losses due to polarization. Specifically, in Tests 1 and 2, minimal differences in RTE are observed across the four cell types. As the testing current density or voltage limits increase, RTE decreases, following the trend: Test 1 > Test 2 > Test 3 > Test 5. In Test 3, UCCA demonstrates the highest and most stable RTE throughout the cycling process. Conversely, cells with cathode coating (CCUA & CCCA) exhibit a rapid decline in RTE within the first 100 cycles, followed by a slight increase and subsequent stabilization in later cycles. Particularly, CCCA consistently outperforms CCUA in RTE. UCUA, on the other hand, experiences a continual decrease in RTE over 1000 cycles. These findings reinforce the earlier conclusion that, under fast-charging conditions, cathode ALD coating accelerates electrode degradation due to increased internal resistance introduced by the insulting the Al_2O_3 layer, while anode ALD coating (thinner than cathode) offers protective benefits during fast charging. In Test 5, CCCA maintains the highest and most stable RTE across 1000 cycles, aligning well with the average voltage difference and cycling performance tests. This further confirms the advantage of ALD coating, whether on the anode or cathode, in enhancing performance during high-voltage cycling.

IV. Postmortem analysis

To better understand the impact of ALD coating on cycling stability and performance at high rates and voltages, after electrochemical testing, all the cells were disassembled in a glove box and rinsed with DMC three times for further characterization. The corresponding optical images of anodes and cathodes for four cell configurations are displayed in Figure 4.

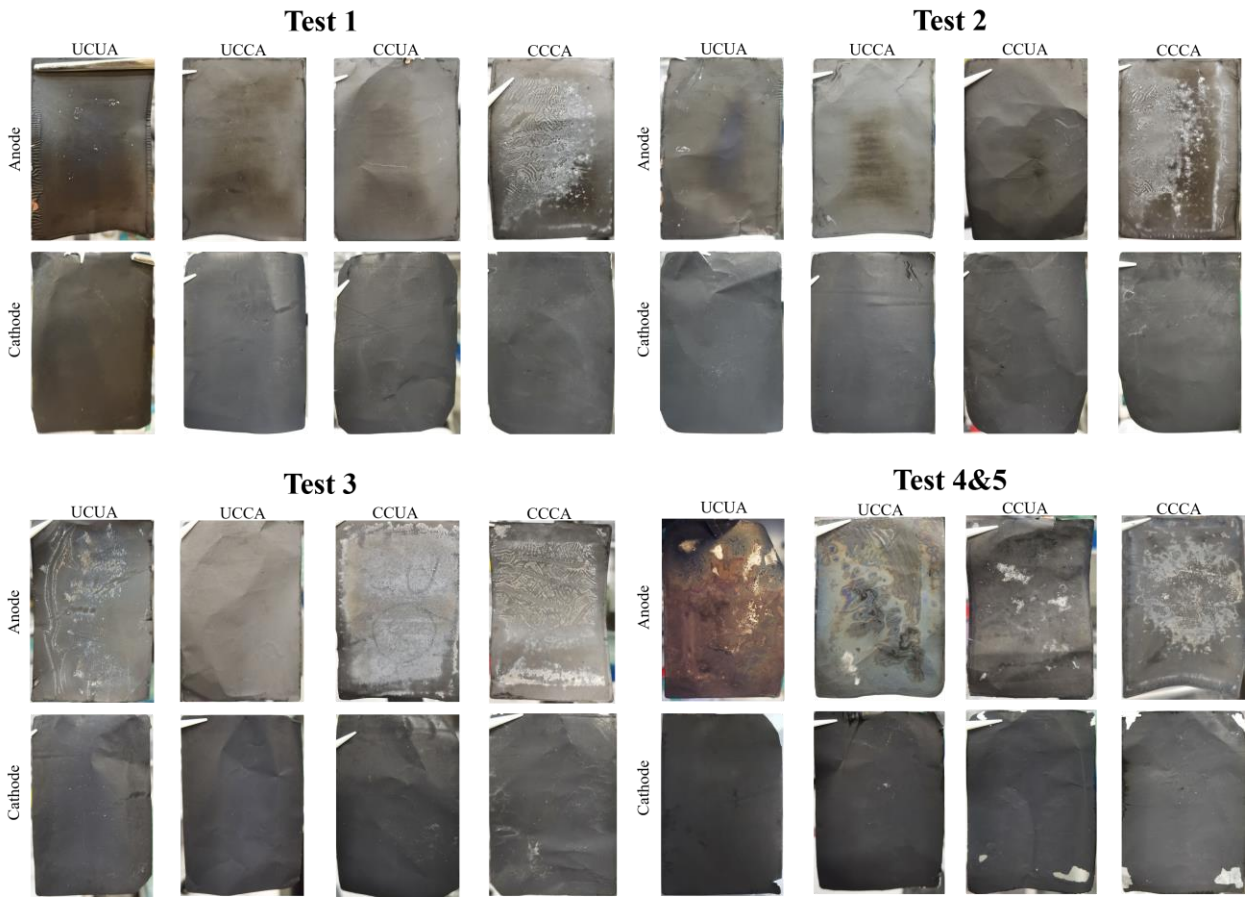

Figure 4. Optical images of anodes and cathodes dissembled from pouch cells with four different configurations after long-term cycling (1,000 cycles) under testing protocols 1-5. All the cells are dissembled in the glove box and rinsed with DMC for 3 times.

Test 1 and Test 2: at relatively low C-rate

Regarding the anodes, white residues, often indicative of lithium plating, are visible on their surfaces in most cases. This plating is confirmed by SEM and EDX analyses. As illustrated in Figure S3, SEM and EDX mapping were conducted on the UCUA anode post-Test 1, focusing on areas both with (c, d) and without (a, b) white residue. In areas with residue, distinct lithium plating structures are evident, as presented in Figure S3 d-1. Additionally, the corresponding EDX mapping (Figure S3 d-2) reveals a high intensity of oxygen at these locations, which could come from the oxidized lithium. In both Tests 1 and 2, lithium plating is shown on both UCUA and CCCA cells. Optical observations suggest more extensive lithium plating in CCCA compared to UCUA, with more white lithium plating presenting on the anode surface. However, a closer examination

at the micro-scale reveals a somewhat different picture. Figure 5 presents SEM images highlighting the lithium plating regions on the anode for UCUA (a, c) and CCCA (b, d) following Tests 1 (a, b) and 2 (c, d). In UCUA, images a-1 and c-1 reveal a tendency for lithium plating to be more localized and concentrated. Conversely, lithium plating on CCCA appears more evenly across the anode, as shown in images b-1 and d-1. Upon closer examination of the lithium plating structures, UCUA exhibits a mossy, thick, and dense morphology. In contrast, CCCA shows a whisker-like lithium plating. Using the same electrolyte and cycling conditions, it's evident that the lithium plating's morphology is significantly influenced by current density [58-61], with mossy structures typically forming at higher densities compared to whisker-like structures [60]. Even though the ALD coating on both the anode and cathode increases material resistance and consequently increases lithium plating, the overpotential across CCCA anode is more evenly distributed compared to that of UCUA. The anodes of UCCA and CCUA were also thoroughly characterized using SEM, as shown in Figure S4. In line with optical observations, no lithium plating is detected on UCCA and CCUA after Tests 1 and 2, as evident in images a-1, b-1, c-1, and d-1. Additionally, under higher magnification views a-2, b-2, c-2, and d-2, neither cracks nor delamination are observed in any of the anodes. Extensive EDX mapping was conducted on all the anodes after Test 1 and 2, over a 420*280 μm² area, with the corresponding elemental analysis presented in Figure S4e and f. Notably, UCUA and CCCA exhibit lower C and higher O levels, signifying relatively higher lithium plating on the anodes. Similar percentages of C, O, F, and P in UCCA and CCUA suggest a comparable extent of SEI formation in these two anodes.

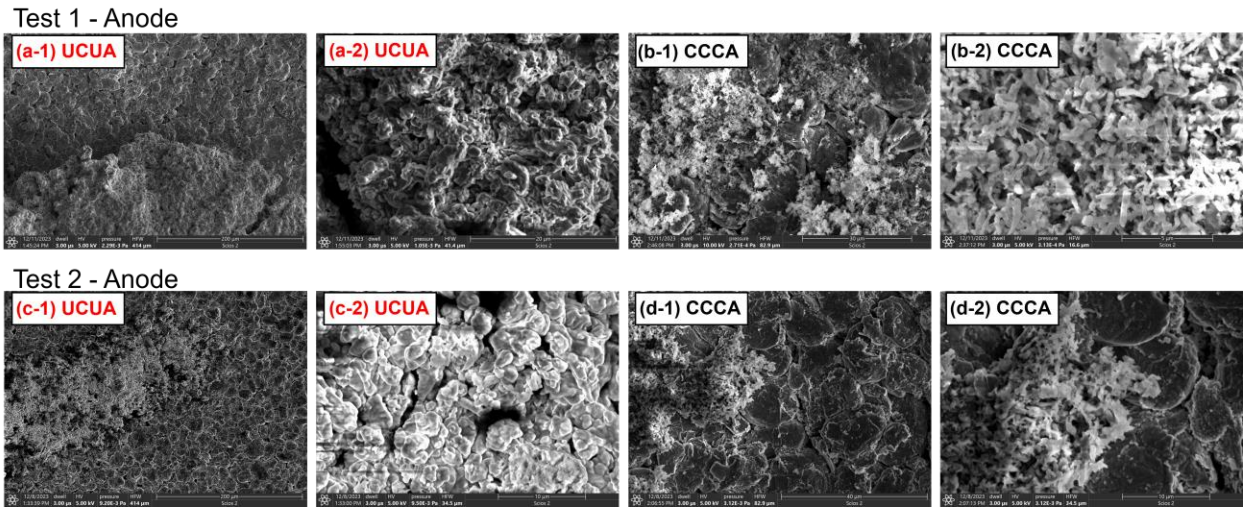

Figure 5. SEM analyses of the anode surface of UCUA (a, c) and CCCA (b, d) Cells post Test 1 (a, b) and Test 2 (c, d). The electrode was disassembled in a glove box and rinsed three times with DMC. Images a2, b2, c2, and d2 offer magnified views of areas with lithium plating.

The cathodes display a similar appearance in optical images across all cells. This similarity persists under SEM characterization, with no notable differences in cathodes among four cell configurations in Tests 1 and 2, as illustrated in Figure S5. To delve deeper into the structural changes and degradation of cathode materials post-cycling, all disassembled cathodes were analyzed using XRD and EDX mapping (covering a 420 x 280 μm² area), as shown in Figure 6. After 1000 cycles across various tests, all cathodes retain good crystallinity without the presence of other phases, such as spinel or rock-salt, being identified. The XRD patterns, particularly at peaks (108)/(110) and (113) of all cycled cathodes, are compared in Figure 6a-d, alongside two pristine reference cathodes (ALD-coated and uncoated NMC 811). Relative to pristine cathodes, an increase in the splitting of (108) and (110) peaks, and a shift of (113) to higher angles are observed in all cycled cathodes. This change suggests lattice shrinkage along *a* and *b* directions and expansion along the *c* direction [62-65], indicative of Li loss in the aged NMC materials. Such alterations impact the interlayer spacing and lattice parameters, reflecting the aging process of cathodes. In Test 1, the UCUA cathode exhibits more pronounced splitting and shifting compared to the others. Additionally, higher carbon and lower oxygen percentages are detected in the UCUA cathode, as shown in Figure 6e. These findings suggest, without any ALD coating on the electrode, greater structural degradation and CEI formation in the UCUA cathode relative to others. Upon comparing Tests 1 and 2, Test 2 reveals more significant splitting and shifting, alongside higher carbon and lower oxygen percentages on the electrode surface. This suggests a more severe structural degradation of the cathode under higher cycling C-rates.

Under low C-rates, despite little differences in cycling performance among all cell configurations, varying levels of degradation are evident in the cycled electrodes. The UCUA cell, without ALD coating, exhibits localized and dense mossy lithium plating on the anode, alongside relatively severe structural degradation and thicker CEI on the cathode. In contrast, cells with ALD coating on either the anode or cathode alone (CCUA and UCCA) display relatively milder degradation on both electrodes. The CCCA cell, with ALD coating on both anode and cathode, experiences increased lithium plating on the anode, yet this plating is more evenly distributed across the anode surface compared to UCUA.

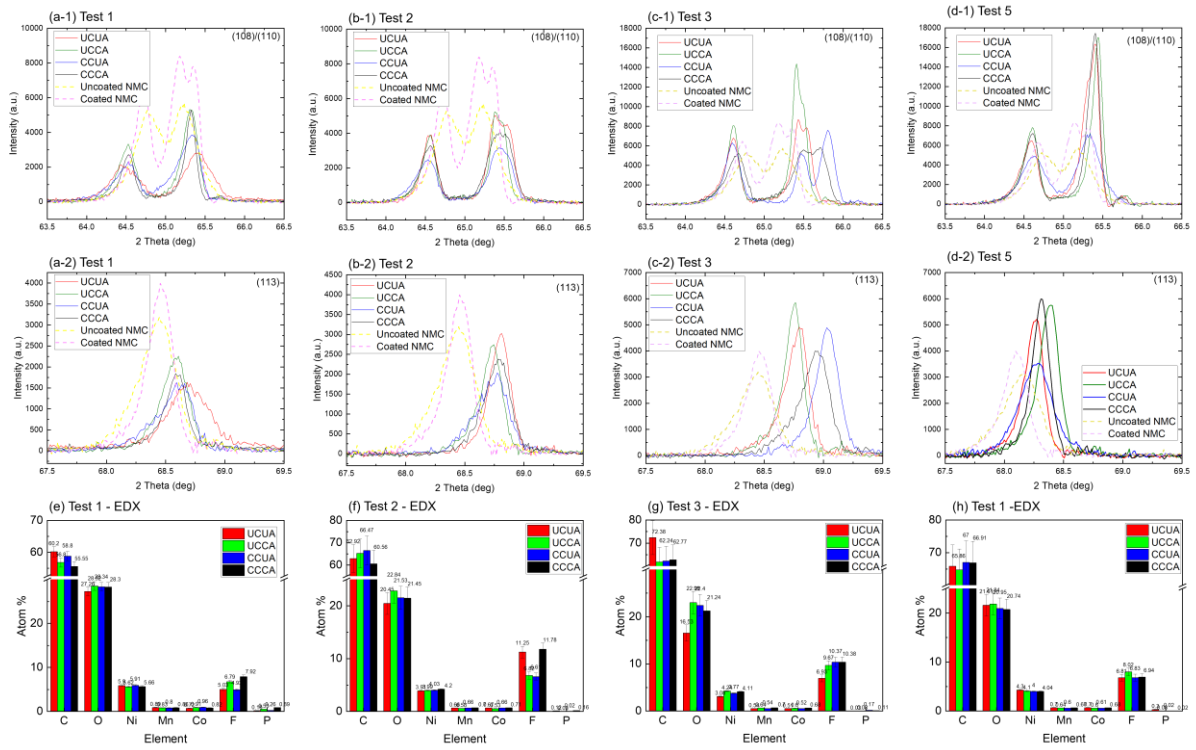

Figure 6. Figure a, b, c, and d display XRD analysis of cycled and pristine cathode materials for Tests 1, 2, 3, and 5, respectively. Figure e, f, g, and h present elemental analysis of the cycled cathode surfaces through EDX mapping for Tests 1, 2, 3, and 5, respectively.

Test 3 – Fast charging

Under fast-charging conditions, ALD coating significantly affects electrode degradation more than at low C-rates. Optical images in Figure 5 show lithium plating on UCUA, CCUA, and CCCA anodes, but not on UCCA. Notably, CCUA anode displays the most extensive lithium plating, almost entirely covering its surface. SEM analysis in Figure 8a-d offers a more detailed view of the anode surface after Test 3. In Figure 7c-1, lithium plating covers the entire CCUA anode surface, with scarcely any visible graphite upon closer inspection (Figure 7c-2). UCUA and CCCA anodes anode surfaces are partially covered with lithium plating (Figure 7a-1, d-1). Zooming in on less plated areas (Figure 7a-2 and d-2) shows graphite still slightly covered by lithium plating and electrolyte decomposition products. Conversely, UCCA shows a clearer graphite surface (Figure 7b), indicating that the full cells with ALD coating solely on anodes exhibit reduced lithium plating under fast charging conditions.

The SEM images in Figure 7 e-f show the cathode surface structures post-Test 3. No big difference can be observed among the cathodes at the particle level. However, more cracks are observed on the CCUA cathode at the electrode level, as marked by the red dash line in Figure 8g-1 and g-2, implying more mechanical stress is introduced in the CCUA cathode during cycling compared to others. In the XRD patterns (Figure 6c), the trend in peak splitting at (108)/(110) and shift at (113) is as follows: CCUA > CCCA > UCUA > UCCA. This suggests that CCUA experiences the most severe cathode degradation, while UCCA exhibits the least. Examining the elemental distribution on the cathode surface, the UCUA cathode displays relatively higher carbon and lower oxygen, nickel, manganese, and cobalt levels, indicative of a thicker CEI layer formation.

Consistent with cycling performance results, under fast-charging conditions, ALD coating on the anode protects both electrodes. It reduces lithium plating and interfacial resistance, thereby lowering heating and increasing the safety of the cell. In contrast, ALD coating on the cathode tends to exacerbate the degradation of both the anode and cathode.

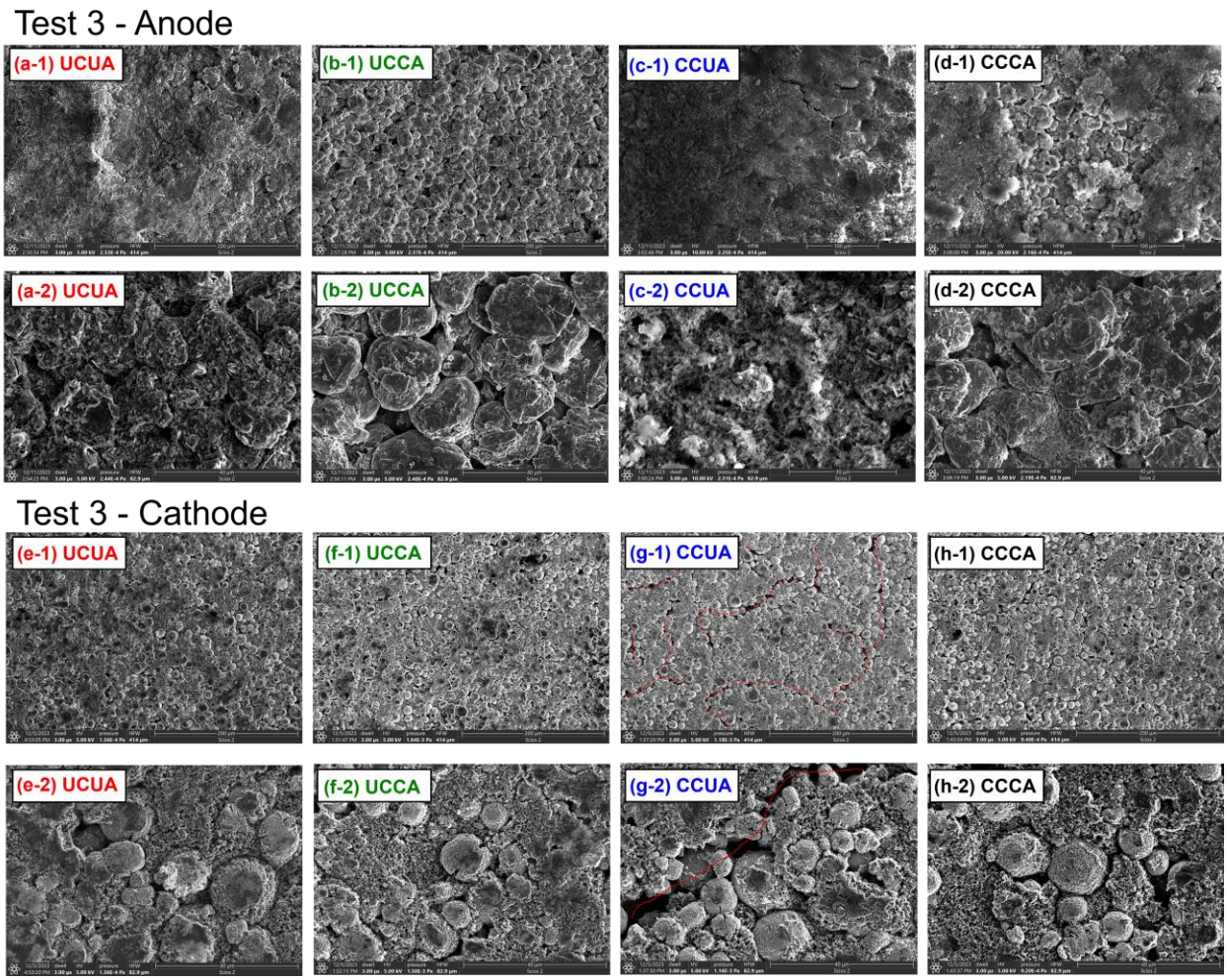

Figure 7. SEM analyses of the anode and cathode surface of four configuration Cells post Test 3. The electrode was disassembled in a glove box and subsequently rinsed three times with DMC.

Test 4&5 – High voltage testing

After high-voltage testing, SEM reveals no significant structural differences in the cathodes, as depicted in Figures S5i-l. The XRD patterns (Figure 6d) show the following trend in peak splitting at (108)/(110) and shift at (113): UCCA > CCCA > UCUA > CCUA, suggesting that ALD coating on the cathode more effectively protects against structural degradation and Li loss of cathodes under high voltage conditions.

Optical (Figure 5) and SEM (Figure 8a-1 to d-1) images reveal lithium plating on all anode surfaces. Localized plating is noted on UCUA, UCCA, and CCUA, with UCUA exhibiting the most severe plating and UCCA the least. Specifically, light lithium plating on UCCA is shown only in one place, while the remainder of the surface remains distinctly clear (Figure 8b-1), indicating that anode-only coating is particularly effective in minimizing lithium plating. Compared to others. CCCA features a more uniform lithium plating distribution, consistent with its appearance in Tests 1-3. Unlike other tests, colorful residues are found in the UCUA and UCCA anodes, as shown in the optical images (Figure 5). These colorful residues are attributed to transition metal deposits, originating from the cathode under high voltage, as confirmed by SEM and EDX characterizations. In Figure 8a-2, brain-shaped deposits, distinct from lithium dendrites, are observed on the UCUA anode. A detailed view of this structure with EDX mapping is provided in Figure 8e-i, where a high Ni intensity is noted on these deposits (Figure 8h). The EDX spectrum (Figure 8i) shows distinct Ni, Co, and Mn peaks, with Ni atomic percentage at 2.96%, significantly higher than the surface average of 0.25% (Figure 8j). Similar deposits are seen on UCCA (Figure 8b-2), but not on CCUA (Figure 8c-2) or CCCA (Figure 8d-2). EDX mapping of the four anodes (over a 420*280 μm² area) reveals higher transition metal intensity under high voltage testing compared to other test protocols, particularly on cells with uncoated cathodes (UCUA, UCCA), indicating more dissolution and deposition of transition metals. This aligns with SEM observations. Among all of them, the CCCA shows the lowest transition metals. All these observations suggest that ALD coating on the cathode more effectively prevents transition metal dissolution under high voltage.

During the high-voltage test, ALD coating on both the anode and cathode notably enhances electrode protection from degradation. Specifically, anode ALD coating helps curb lithium plating, while cathode ALD coating effectively minimizes transition metal dissolution.

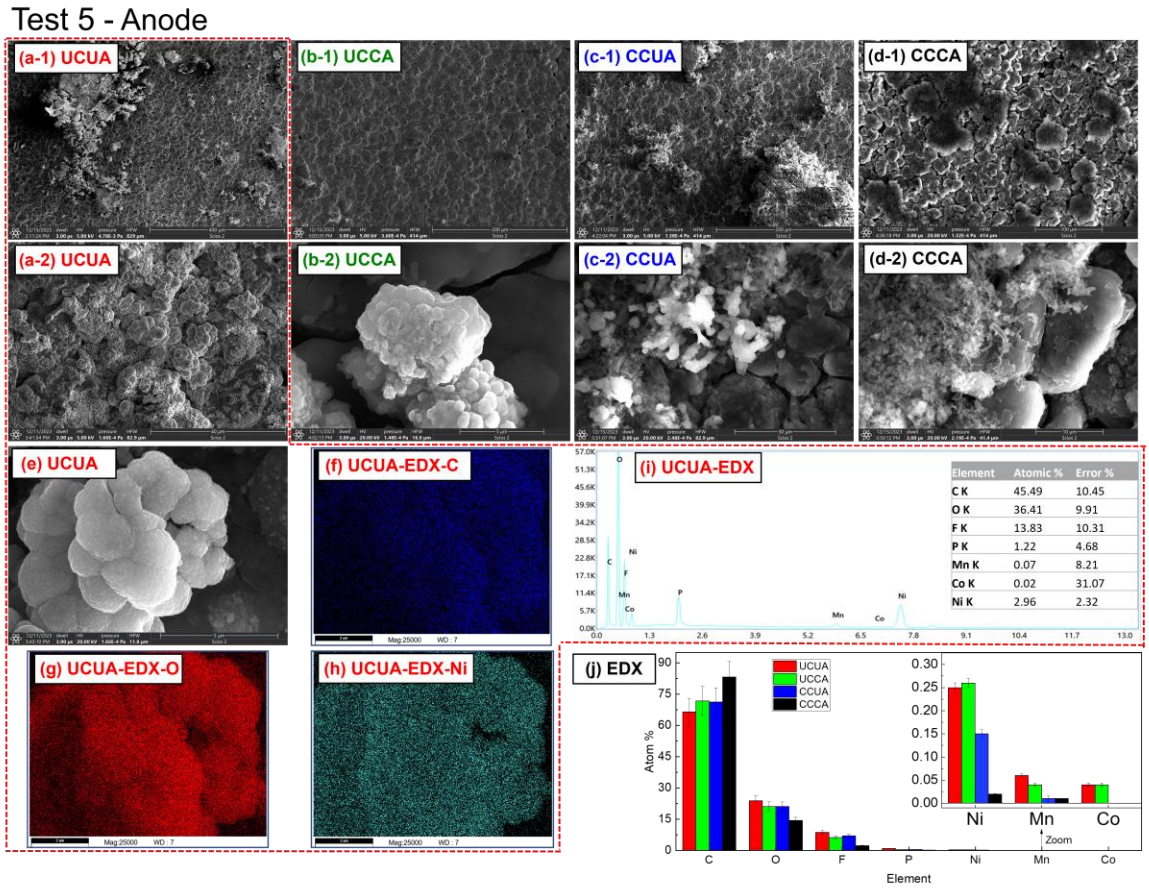

Figure 8. SEM and EDX Analyses of Anodes from Four Cell Configurations Post Test 5. The electrodes, disassembled and rinsed in a glove box with DMC, are illustrated as follows: Figures (a-1) to (d-1) display wide views of the electrode surfaces. Figures (a-2) to (d-2) offer zoomed-in views on the metal plating areas. A brain-structured metal plating on the UCUA anode is captured in (e), with corresponding EDX elemental mapping in (f) for Carbon, (g) for Oxygen, and (h) for Nickel. The associated EDX spectrum is detailed in panel (i). Comprehensive element analysis of the cycled anodes from the four configurations, as determined by EDX mapping, is shown in (j).

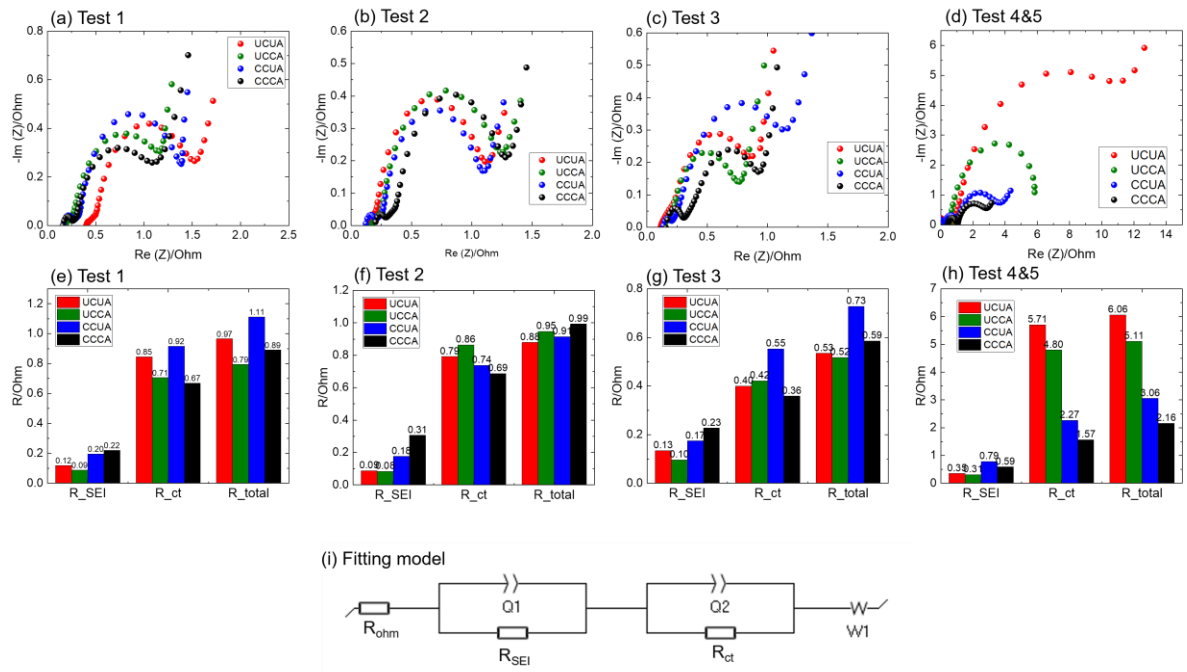

Figure 9. Nyquist plots and fitted R_{SEI} and R_{ct} values from four-configuration cells after 1,000 cycles, tested under protocols 1 (a-b), 2 (c-d), 3 (e-f), and 5 (g-h). (i) Equivalent circuit model used for impedance fitting.

The resulting Nyquist plots for the four cell configurations after Tests 1, 2, 3, and 5 are presented in Figure 9a-d. For a more accurate assessment of the internal resistance of each cell, the EIS data were analyzed using an equivalent circuit model, as shown in Figure 9i. The extracted parameters, including solid electrolyte interphase resistance (R_{SEI}), charge transfer resistance (R_{ct}), and their aggregate (R_{total}) are detailed in Figures 9e-h. R_{ohm} is excluded due to minor variations arising from unstable connections between the cell and the cell holder during measurement. The variance among the four cells is less pronounced in Test 1 and 2 compared to Test 3 and 5, correlating well with their cycling performance - no big difference under small C-rate. In both Test 1 and Test 2, CCCA shows a relatively higher R_{SEI}, which shows a good agreement as the teardown observation – obvious white residue on CCCA surface in Test 1 and Test 2. The more serious electrolyte decomposition and Lithium plating on the CCCA anode surface could be caused by higher resistance introduced by the ALD coating on both the anode and cathode particles. Following the fast charge testing (Test 3), CCUA exhibited the highest total resistance, resulting from significant lithium plating on the anode and considerable cathode degradation. Conversely, UCCA displayed the lowest total resistance, attributable to its minimal electrode degradation. This finding reinforces that under fast charging conditions, ALD coating on the

cathode hastens battery aging, whereas ALD coating on the anode enhances overall cell performance. Under high voltage test, UCUA registers the highest total resistance, caused by severe lithium and transition metal plating on the anode and cathode metal dissolution. Cells with uncoated cathodes (UCUA & UCCA) exhibit relatively high R_{ct}, attributed to significant transition metal dissolution in the absence of ALD coating. Conversely, CCCA demonstrates the lowest resistance, due to its minimal transition metal dissolution and comparatively uniform lithium plating.

5. Conclusions

To bridge the gap between laboratory achievements and the commercialization of ALD-coated battery materials, this study comprehensively evaluated the effects of commercially scalable Al_2O_3 ALD coatings on anode and cathode powders in full pouch cells, across various operational conditions: long-term cycling, fast discharge, fast charging, and high-voltage testing. It was observed that in cycling performance Test 1 and Test 2 (at lower voltage and C-rates < ~1C), the impact of ALD coating on cell performance was not significant – the cycling performance was equivalent. Moreover, most of these cells (24 in total) can maintain a discharge capacity above 140 mAh/g after 1,000 cycles and approximately 80% capacity retention after cycling, indicating high quality and good consistency of all the pouch cells. Under fast charging conditions at 4C, ALD coating on the anode positively influenced cell performance by providing a protection layer on the anode, while the coating on the cathode presented drawbacks, potentially due to resistance increased by introducing the insulating Al_2O_3 layer. In the leakage current test (4.6V for 2 days) and high-voltage test (4.4V), increased metal dissolution was noted on all cells compared to the other lower voltage tests. However, the application of ALD coating on either the anode or cathode effectively minimizes side reactions on the electrodes at high voltages, consequently enhancing cell performance. Overall cell performance evaluation indicated that UCCA cells exhibited impressive performance, especially in fast charge tests, while CCCA cells maintained consistent performance across various testing conditions, although they experienced more lithium plating at lower C-rates compared to other cell configurations. This comprehensive study not only confirms the viability of ALD coatings in enhancing LIB performance under various testing conditions but also highlights the critical role of scalable ALD technology in advancing the development of a safer, more efficient, and economically feasible LIB manufacturing approach.

Author Contributions

Y. F. contributed to the experiment design, experimental results, data analysis, and original paper writing. R. T. contributed to some SEM characterizations and paper editing. K. L. contributed to the electrode coatings, cell assembling and testing. J. S. participated in the TEM-EDX analysis and paper editing. D. C. performed the TEM-EDX characterizations. Y. L. performed the XRD characterizations. W. S. contributed to cell assembling and testing. M. G. contributed to the conception, ALD coating, ICP-OPS characterization, and paper writing. A. D. contributed to the conception, experiment design, and paper editing. G. P. contributed to the conception and paper editing. J.L. contributed to conception, experiment design, data analysis, and paper editing.

ACKNOWLEDGMENTS

This research at Oak Ridge National Laboratory, managed by UT Battelle LLC, for the US Department of Energy (DOE), was sponsored by the Advanced Materials and Manufacturing Technologies Office (Program Managers: Changwon Suh). This research used the resources of the Center for Nanophase Materials Sciences (CNMS) which is DOE Office of Science User Facilities.

References

1. Radin, M.D., et al., *Narrowing the Gap between Theoretical and Practical Capacities in Li-Ion Layered Oxide Cathode Materials.* Advanced Energy Materials, 2017. **7**(20): p. 1602888.
2. Sun, T., et al., *A Biodegradable Polydopamine-Derived Electrode Material for High-Capacity and Long-Life Lithium-Ion and Sodium-Ion Batteries.* Angewandte Chemie International Edition, 2016. **55**(36): p. 10662-10666.
3. Weiss, M., et al., *Fast Charging of Lithium-Ion Batteries: A Review of Materials Aspects.* Advanced Energy Materials, 2021. **11**(33): p. 2101126.
4. Yang, X.-G., et al., *Fast charging of lithium-ion batteries at all temperatures.* Proceedings of the National Academy of Sciences, 2018. **115**(28): p. 7266-7271.
5. Hu, M., X. Pang, and Z. Zhou, *Recent progress in high-voltage lithium ion batteries.* Journal of Power Sources, 2013. **237**: p. 229-242.
6. Kim, J.-H., N.P.W. Pieczonka, and L. Yang, *Challenges and Approaches for High-Voltage Spinel Lithium-Ion Batteries.* ChemPhysChem, 2014. **15**(10): p. 1940-1954.
7. Li, J., et al., *Toward Low-Cost, High-Energy Density, and High-Power Density Lithium-Ion Batteries.* JOM, 2017. **69**(9): p. 1484-1496.

8. Wang, H.-G., et al., *Electrospun materials for lithium and sodium rechargeable batteries: from structure evolution to electrochemical performance.* Energy & Environmental Science, 2015. **8**(6): p. 1660-1681.
9. Hausbrand, R., et al., *Fundamental degradation mechanisms of layered oxide Li-ion battery cathode materials: Methodology, insights and novel approaches.* Materials Science and Engineering: B, 2015. **192**: p. 3-25.
10. He, W., et al., *Challenges and Recent Advances in High Capacity Li-Rich Cathode Materials for High Energy Density Lithium-Ion Batteries.* Advanced Materials, 2021. **33**(50): p. 2005937.
11. Nie, K., et al., *Interfaces Between Cathode and Electrolyte in Solid State Lithium Batteries: Challenges and Perspectives.* Frontiers in Chemistry, 2018. **6**.
12. Asenbauer, J., et al., *The success story of graphite as a lithium-ion anode material – fundamentals, remaining challenges, and recent developments including silicon (oxide) composites.* Sustainable Energy & Fuels, 2020. **4**(11): p. 5387-5416.
13. An, S.J., et al., *The state of understanding of the lithium-ion-battery graphite solid electrolyte interphase (SEI) and its relationship to formation cycling.* Carbon, 2016. **105**: p. 52-76.
14. Kaliaperumal, M., et al. *Cause and Mitigation of Lithium-Ion Battery Failure—A Review*. Materials, 2021. **14**, DOI: 10.3390/ma14195676.
15. Wang, Q., et al., *A review of lithium ion battery failure mechanisms and fire prevention strategies.* Progress in Energy and Combustion Science, 2019. **73**: p. 95-131.
16. Tranquillo, E. and F. Bollino, *Surface Modifications for Implants Lifetime extension: An Overview of Sol-Gel Coatings.* Coatings, 2020. **10**(6): p. 589.
17. Feng, T., et al., *Low-Cost Al_2O_3 Coating Layer As a Preformed SEI on Natural Graphite Powder To Improve Coulombic Efficiency and High-Rate Cycling Stability of Lithium-Ion Batteries.* ACS Applied Materials & Interfaces, 2016. **8**(10): p. 6512-6519.
18. Smaldone, A., et al., *Iron doped LiCoPO4 thin films for lithium-ion microbatteries obtained by ns pulsed laser deposition.* Applied Surface Science, 2018. **445**: p. 56-64.
19. Kim, D., et al., *Carbon-coated SiOx anode materials via PVD and pyrolyzed fuel oil to achieve lithium-ion batteries with high cycling stability.* Carbon Letters, 2022. **32**(1): p. 321-328.
20. Fu, K., et al., *Effect of CVD carbon coatings on Si@CNF composite as anode for lithium-ion batteries.* Nano Energy, 2013. **2**(5): p. 976-986.
21. Kim, B.-R., J.-H. Kim, and J.-S. Im, *Effect and Mechanism of Pitch Coating on the Rate Performance Improvement of Lithium-Ion Batteries.* Materials, 2022. **15**(13): p. 4713.
22. Dahmen, K.-H., *Chemical Vapor Deposition*, in *Encyclopedia of Physical Science and Technology (Third Edition)*, R.A. Meyers, Editor. 2003, Academic Press: New York. p. 787-808.
23. Karimzadeh, S., et al., *Emerging Atomic Layer Deposition for the Development of High-Performance Lithium-Ion Batteries.* Electrochemical Energy Reviews, 2023. **6**(1).
24. George, S.M., *Atomic Layer Deposition: An Overview.* Chemical Reviews, 2010. **110**(1): p. 111-131.
25. Meng, X., *Atomic and molecular layer deposition in pursuing better batteries.* Journal of Materials Research, 2021. **36**: p. 2-25.
26. David, L., et al., *Unveiling the Role of Al_2O_3 in Preventing Surface Reconstruction During High-Voltage Cycling of Lithium-Ion Batteries.* ACS Applied Energy Materials, 2019. **2**(2): p. 1308-1313.
27. Young, M.J., et al., *High-Rate Spinel LiMn2O4 (LMO) Following Carbonate Removal and Formation of Li-Rich Interface by ALD Treatment.* The Journal of Physical Chemistry C, 2019. **123**(39): p. 23783-23790.

28. Wise, A.M., et al., *Effect of Al2O3 coating on stabilizing LiNi0. 4Mn0. 4Co0. 2O2 cathodes.* Chemistry of Materials, 2015. **27**(17): p. 6146-6154.
29. Lu, S., et al., *Atomic layer deposition of ZnO on carbon black as nanostructured anode materials for high-performance lithium-ion batteries.* Nanoscale, 2017. **9**(3): p. 1184-1192.
30. Liu, Y., et al., *Atomic-scale tuned interface of nickel-rich cathode for enhanced electrochemical performance in lithium-ion batteries.* Journal of Materials Science & Technology, 2020. **54**: p. 77-86.
31. Tiurin, O., et al., *Atomic layer deposition (ALD) of lithium fluoride (LiF) protective film on Li-ion battery LiMn1.5Ni0.5O4 cathode powder material.* Journal of Power Sources, 2020. **448**: p. 227373.
32. Zhou, Y., et al., *Coating Solution for High-Voltage Cathode: AlF3 Atomic Layer Deposition for Freestanding LiCoO2 Electrodes with High Energy Density and Excellent Flexibility.* ACS Applied Materials & Interfaces, 2017. **9**(11): p. 9614-9619.
33. Kim, J.W., et al., *Unexpected high power performance of atomic layer deposition coated Li [Ni1/3Mn1/3Co1/3] O2 cathodes.* Journal of Power Sources, 2014. **254**: p. 190-197.
34. Jung, Y.S., et al., *Enhanced Stability of LiCoO[sub 2] Cathodes in Lithium-Ion Batteries Using Surface Modification by Atomic Layer Deposition.* Journal of The Electrochemical Society, 2010. **157**(1): p. A75.
35. Jung, Y.S., et al., *Ultrathin Direct Atomic Layer Deposition on Composite Electrodes for Highly Durable and Safe Li-Ion Batteries.* Advanced Materials, 2010. **22**(19): p. 2172-2176.
36. Dahlberg, K., et al. *ALD-Coated Graphite Anode Materials for Improved Cycle Life, Calendar Life, and Safety of Li-Ion Cells*. in *Electrochemical Society Meeting Abstracts 232*. 2017. The Electrochemical Society, Inc.
37. Tian, R., et al., *Low-Weight 3D Al2O3 Network as an Artificial Layer to Stabilize Lithium Deposition.* ChemSusChem, 2018. **11**(18): p. 3243-3252.
38. Hy, S., et al., *Stabilizing nanosized Si anodes with the synergetic usage of atomic layer deposition and electrolyte additives for Li-ion batteries.* ACS applied materials & interfaces, 2015. **7**(25): p. 13801-13807.
39. Hsieh, C.-T., et al., *Roll-to-roll atomic layer deposition of titania nanocoating on thermally stabilizing lithium nickel cobalt manganese oxide cathodes for lithium ion batteries.* ACS Applied Energy Materials, 2020. **3**(11): p. 10619-10631.
40. Li, J., et al., *Evaluation Residual Moisture in Lithium-Ion Battery Electrodes and Its Effect on Electrode Performance.* MRS Advances, 2016. **1**(15): p. 1029-1035.
41. An, S.J., et al., *Correlation of electrolyte volume and electrochemical performance in lithium-ion pouch cells with graphite anodes and NMC532 cathodes.* Journal of The Electrochemical Society, 2017. **164**(6): p. A1195.
42. Märker, K., et al., *Evolution of Structure and Lithium Dynamics in $LiNi_{0.8}Mn_{0.1}Co_{0.1}O_2$ (NMC811) Cathodes during Electrochemical Cycling.* Chemistry of Materials, 2019. **31**(7): p. 2545-2554.
43. Lipson, A.L., et al., *Stabilizing NMC 811 Li-Ion Battery Cathode through a Rapid Coprecipitation Process.* ACS Applied Energy Materials, 2021. **4**(2): p. 1972-1977.
44. Lu, X., et al., *Improved Capacity Retention of SiO2-Coated LiNi0.6Mn0.2Co0.2O2 Cathode Material for Lithium-Ion Batteries.* Applied Sciences, 2019. **9**(18): p. 3671.
45. Sharma, J., et al., *Enhancing the Electrochemical Performance of Aqueous Processed Li-Ion Cathodes with Silicon Oxide Coatings.* ChemSusChem, 2023. **16**(16): p. e202300350.
46. Young, M.J., et al., *Probing the atomic-scale structure of amorphous aluminum oxide grown by atomic layer deposition.* ACS applied materials & interfaces, 2020. **12**(20): p. 22804-22814.

47. Phattharasupakun, N., et al., *Effect of charging protocols on electrochemical performance and failure mechanism of commercial level Ni-rich NMC811 thick electrode.* Electrochemistry Communications, 2022. **139**: p. 107309.
48. Severson, K.A., et al., *Data-driven prediction of battery cycle life before capacity degradation.* Nature Energy, 2019. **4**(5): p. 383-391.
49. Gyenes, B., et al., *Understanding Anomalous Behavior in Coulombic Efficiency Measurements on Li-Ion Batteries.* Journal of The Electrochemical Society, 2015. **162**(3): p. A278-A283.
50. Lewerenz, M., et al., *Systematic aging of commercial LiFePO4|Graphite cylindrical cells including a theory explaining rise of capacity during aging.* Journal of Power Sources, 2017. **345**: p. 254-263.
51. Dubarry, M., C. Truchot, and B.Y. Liaw, *Synthesize battery degradation modes via a diagnostic and prognostic model.* Journal of Power Sources, 2012. **219**: p. 204-216.
52. Kobayashi, Y., et al., *Unexpected capacity fade and recovery mechanism of LiFePO4/graphite cells for grid operation.* Journal of Power Sources, 2020. **449**: p. 227502.
53. Guo, J., et al., *Understanding the mechanism of capacity increase during early cycling of commercial NMC/graphite lithium-ion batteries.* Journal of Energy Chemistry, 2022. **74**: p. 34-44.
54. Davoodabadi, A., et al., *On electrolyte wetting through lithium-ion battery separators.* Extreme Mechanics Letters, 2020. **40**: p. 100960.
55. Kawabata, K., et al., *Fluidity of a slurry of the graphite powder coated with Al2O3-based metal oxides.* Journal of materials science letters, 2001. **20**: p. 851-853.
56. Kim, D.S., Y.E. Kim, and H. Kim, *Improved fast charging capability of graphite anodes via amorphous Al2O3 coating for high power lithium ion batteries.* Journal of power sources, 2019. **422**: p. 18-24.
57. Li, J., et al., *Reduction of surface residual lithium compounds for single-crystal LiNi0. 6Mn0. 2Co0. 2O2 via Al2O3 atomic layer deposition and post-annealing.* Coatings, 2022. **12**(1): p. 84.
58. Siczek, K.J., *Chapter Eight - Negative Electrode (Anode) Materials*, in *Next-Generation Batteries with Sulfur Cathodes*, K.J. Siczek, Editor. 2019, Academic Press. p. 117-131.
59. Bai, P., et al., *Transition of lithium growth mechanisms in liquid electrolytes.* Energy & Environmental Science, 2016. **9**(10): p. 3221-3229.
60. Frenck, L., et al., *Factors That Control the Formation of Dendrites and Other Morphologies on Lithium Metal Anodes.* Frontiers in Energy Research, 2019. **7**.
61. Ringbeck, F., et al., *Identification of lithium plating in lithium-ion batteries by electrical and optical methods.* Journal of the electrochemical society, 2020. **167**(9): p. 090536.
62. Daemi, S.R., et al., *Exploring cycling induced crystallographic change in NMC with X-ray diffraction computed tomography.* Physical Chemistry Chemical Physics, 2020. **22**(32): p. 17814-17823.
63. Buchberger, I., et al., *Aging Analysis of Graphite/LiNi1/3Mn1/3Co1/3O2 Cells Using XRD, PGAA, and AC Impedance.* Journal of The Electrochemical Society, 2015. **162**(14): p. A2737.
64. Li, J., et al., *In Situ X-ray Diffraction Study of Layered Li–Ni–Mn–Co Oxides: Effect of Particle Size and Structural Stability of Core–Shell Materials.* Chemistry of Materials, 2016. **28**(1): p. 162-171.
65. Weber, R., et al., *Operando X-ray Diffraction Study of Polycrystalline and Single-Crystal $Li_xNi_{0.5}Mn_{0.3}Co_{0.2}O_2$.* Journal of The Electrochemical Society, 2017. **164**(13): p. A2992-A2999.